Chapter 2

Multistrand cables and magnets

A survey of aspects affecting the electrodynamic properties of superconducting cables and magnets

The starting point of this chapter is the general expression for the magnetic field in the aperture of a magnet, which leads to the current distribution for generating a perfect multipole field of the order n. It is shown that, in particular, a perfect dipole field can be approximated by means of a 'shell-type' configuration of multistrand Rutherford-type cables.

The grading of the current density between the inner and outer coils and the structure enclosing the superconducting coils are discussed. Moreover, aspects concerning the operation of magnets such as quenching, training, quench protection, beam losses, operation procedure and operating temperature are dealt with. Those aspects of the cables and magnets that directly influence the electrodynamic behaviour of the magnets are explained in more detail. These are especially: the precompression of the coils, the cable-to-cable connections, the field and stress distribution in the straight part and in the coil ends, the cable geometry, the curing of the cable insulation, the matrix resistivity, the filament size and the twisting of the filaments and strands.

A survey of the dipole model magnets that are investigated at CERN is presented as well as a survey of the main characteristics of the cables from which the coils are wound.

Finally, a general relation between the critical current in a NbTi superconductor and the field and temperature is introduced which is required for the analysis of the ramp-rate induced quenches (chapter 8).

2.1 Magnetic field in the aperture of a magnet

The magnetic field at position $\mathbf{z}=x+iy$ (see Fig. 2.2a) in the aperture of an accelerator magnet is usually expressed as a multipole expansion in two dimensions:

$$\mathbf{B} = B_y + iB_x = \sum_{n=1}^{\infty}(B_n + iA_n)\left((x+iy)/r_0\right)^{n-1} \quad [\mathrm{T}] , \tag{2.1}$$

with r_0 the reference radius (normally $r_0 = 10$ mm) and n the number of the harmonic component. B_n and A_n are called the normal- and skew-multipole coefficients respectively.

A coil, in which only B_1 and A_1 have finite values, while all the higher components ($n > 1$) are zero, is called a dipole coil and has a field:

$$\mathbf{B} = B_1 + iA_1 \quad [\mathrm{T}] . \tag{2.2}$$

In a twin-aperture magnet the A_1 component represents the misalignment between the dipole field of the two coil systems. In the case of single-aperture magnets the coordinate system is often defined in such a way that the average A_1 (along the magnet axis) equals 0 so that **B** corresponds to a normal-dipole field in the y-direction.

A coil in which all multipole fields are zero except for $n=2$ is called a normal quadrupole coil and has a field:

$$\mathbf{B} = B_2\left(\frac{x}{r_0} + i\frac{y}{r_0}\right) + A_2\left(i\frac{x}{r_0} - \frac{y}{r_0}\right) \quad [\mathrm{T}] , \tag{2.3}$$

where the coordinate system is often defined in such a way that the average A_2 is equal to 0. In a similar way sextupole ($n=3$), octupole ($n=4$), decapole ($n=5$) and higher-order coils are defined (note that in the USA $n=0$ is taken as the dipole, $n=1$ the quadrupole and so on).

A perfect multipole field of order n is produced by a current density that varies as a function of the azimuthal angle θ as:

$$J(\theta) = J_0 \cos(n\theta) \quad [\mathrm{Am}^{-2}] . \tag{2.4}$$

The current distributions for a dipole, quadrupole and sextupole field of infinitely long coils are shown in Fig. 2.1.

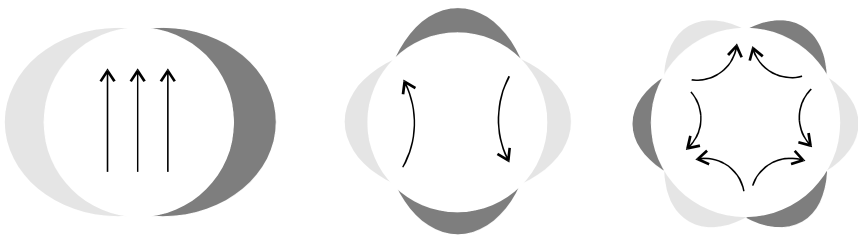

Figure 2.1. Current distributions for generating pure dipole, quadrupole and sextupole fields. The dark and light parts indicate positive and negative current densities respectively. The arrows denote the field direction. The direction of the currents is normal to that of the fields.

Dipole and quadrupole magnets are the main magnetic components of circular accelerators. The function of the main dipole magnets is to keep the beam of accelerated particles on the circular equilibrium orbit, perpendicular to the field direction. The main quadrupole magnets focus and defocus the beam around the equilibrium orbit.

Since a perfect cos($n\theta$) current distribution can never be technically achieved, other multipole components are present which are referred to as distortions or field errors. The distortions are corrected for by using tuning quadrupole-, sextupole- and other higher-order coils. Skew dipole magnets are required for correcting the beam in the vertical plane.

The main multipole is often referred to as the main component or fundamental, while the other multipoles are called harmonics. The harmonics are often normalised to the main component, so, for example, for a dipole coil:

$$\mathbf{B} = B_1 \sum_{n=1}^{\infty} (b_n + ia_n)\big((x+iy)/r_0\big)^{n-1} \quad [\mathrm{T}] \,, \tag{2.5}$$

with:

$$b_n = \frac{B_n}{B_1}, \quad a_n = \frac{A_n}{B_1} \;. \tag{2.6}$$

Design values of b_n and a_n for the lower harmonics of the LHC dipole magnets at injection field $B_{inj} = 0.58$ T (see section 2.2.7) are typically about 10^{-4} at $r_0 = 10$ mm. The relative multipole components b_n and a_n are therefore often expressed in units of 10^{-4}.

2.2 Magnet characteristics

In section 2.1 it is shown that a perfectly homogeneous dipole field is generated by a cos(θ) current distribution, i.e. by a geometry of two intersecting circles or ellipses with their centres spaced apart, and with opposite current direction (see Fig. 2.2a). In practical high-field accelerator magnets such a current distribution can only be approximated since the coils are made from cables. Wide flattened cables carrying high currents are applied in order to limit the inductance and therefore enable a safe quench protection.

Usually, the so called ‘shell-type’ configuration is applied to approximate the ideal cos(θ) distribution. The cross-section of one quadrant of one aperture of a typical LHC dipole magnet is shown in Fig. 2.2b. Quadrants 1 and 2 are also referred to as pole 1 and quadrants 3 and 4 as pole 2. The main advantages of this configuration are that the conductor is put close to the aperture for an efficient use of the superconductor and that the coil ends are formed ‘naturally’ by the Roman-arc geometry. The blocks are separated by copper wedges to have enough design parameters to produce a high-quality dipole field and because the keystone angle of the cable (see eq. 2.14) is not sufficiently large to have radially orientated cables.

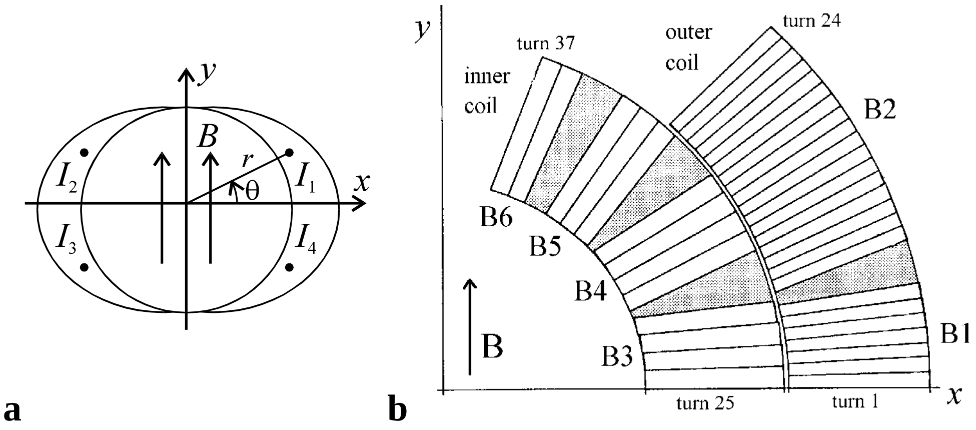

Figure 2.2. **a:** Generation of a perfect dipole field by two intersecting ellipses with their centres spaced apart. I_1 (+), I_2 (-), I_3 (-) and I_4 (+) indicate the currents in the four quadrants at positions (r,θ), $(r, \pi-\theta)$, $(r,\pi+\theta)$ and $(r,-\theta)$ respectively.
b: View of the cross-section of the turns of quadrant 1 of a two-shell dipole (here the design of the Pink Book Dipole magnet -see Table 2.1- is shown) and nomenclature of the blocks and turns (1-24 in the outer coil and 25-37 in the inner coil).

Since the currents in the inner and outer coils are equal while the peak field in the inner coil is larger than that in the outer coil (see also Fig. 2.6), a *grading of the current density* between the two coils is preferable. The grading is obtained by winding the inner and outer coils from cables with a different cross-section. Hence, three different *cable-to-cable connections* are present:

- Connections between the two coils of the same pole, also called splices. Each splice is located in a high-field region and is made by soldering the two cables over a length of about 15 cm (see Fig. 2.3). The resistance of the splice is typically 0.2-0.5 nΩ at zero field and increases due to the magnetoresistance with a factor of about 2-4 for a central field of 9 T.
- Connections between the coils of different poles. The connections are located in a low-field region and often shunted by a copper bar which results in a small resistance, normally about 0.2-0.5 nΩ.
- Connections between the current leads and the cables.

Fig. 2.3 shows a longitudinal view of the magnet with the positioning of the turns and the connections. The head of the magnet where the connections are located is referred to as the connection end whereas the opposite end is called the non-connection end.

The field distribution in the coil ends differs considerably from that in the straight part. Since the cable is bent over the beam pipe (see Fig. 2.4), the field $B_\perp$ normal to the large face of the cable reduces to almost zero (see also section 2.2.4). As a result, the interstrand coupling power loss, which is proportional to $\dot{B}_\perp^{\,2}$ (see chapter 4), is strongly reduced in the coil ends. However, the strong variations in $\dot{B}_\perp$ along the cable also cause boundary-induced coupling currents (see chapter 5) which affect the electrodynamic properties of the magnet.

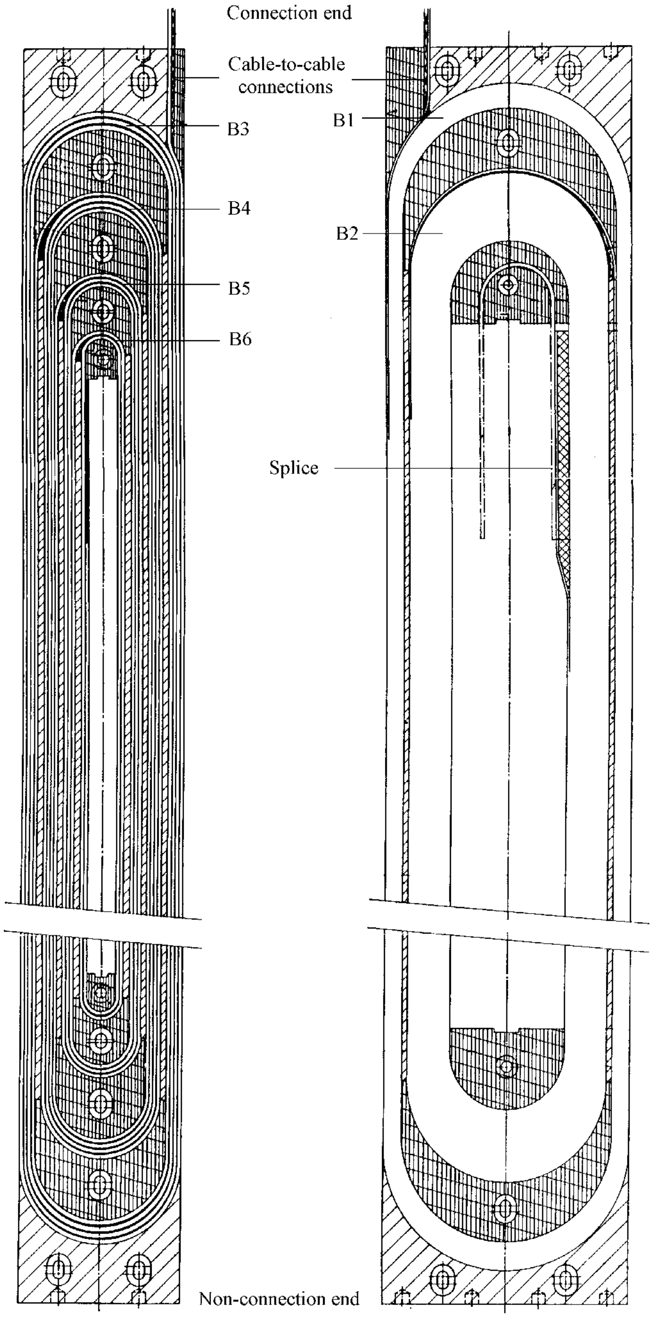

Figure 2.3. Longitudinal view of one pole of a dipole magnet showing the positioning of the turns, the splice between the inner and outer coils, and the connections to the other poles or the current leads. The turns of the outer coil are not drawn individually [LHC, '88].

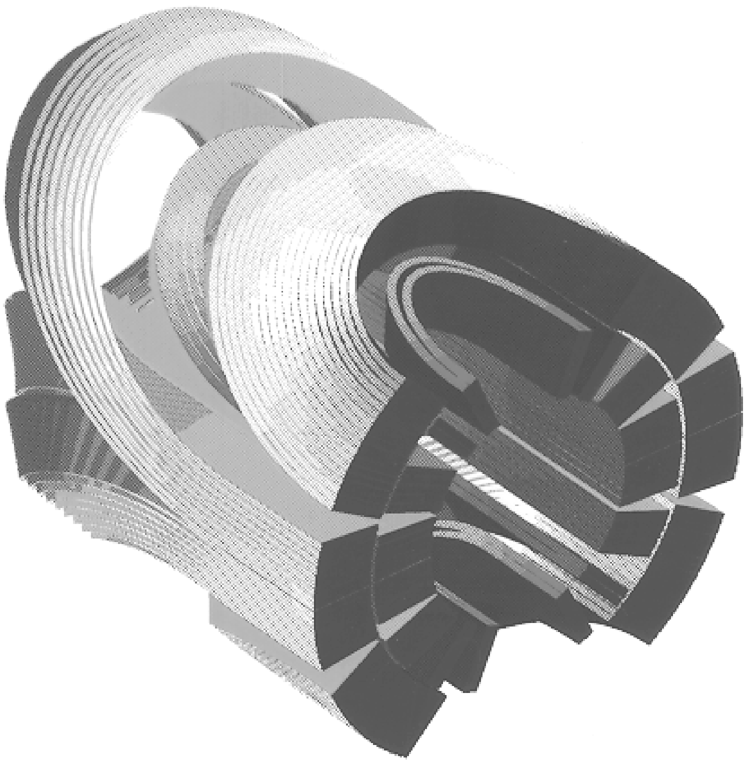

Figure 2.4. 3D view of the turns at the non-connection end of a six-block LHC-type dipole magnet [Russenschuck, '93].

The field at a position $\mathbf{z}=x+iy$ caused by a current I at position $\mathbf{r}=x_1+iy_1$ is, according to the law of Biot and Savart:

$$\mathbf{B}=\frac{\mu_0 I}{2\pi(\mathbf{z}-\mathbf{r})} \quad [\mathrm{T}] . \tag{2.7}$$

A current distribution over the four quadrants in a magnet (see Fig. 2.2a), symbolically represented by:

$$\begin{bmatrix} I_2 & I_1 \\ I_3 & I_4 \end{bmatrix} \text{at} \begin{bmatrix} r,\pi-\theta & r,\theta \\ r,\pi+\theta & r,-\theta \end{bmatrix} \quad , \tag{2.8}$$

can be described by a linear combination of the currents I_A, I_B, I_C and I_D, corresponding to the different harmonic components of eq. 2.5:

$$\begin{bmatrix} -1 & +1 \\ -1 & +1 \end{bmatrix} I_A \qquad \text{normal odd, } B_1, B_3, B_5 \ldots, \tag{2.9}$$

$$\begin{bmatrix} +1 & +1 \\ +1 & +1 \end{bmatrix} I_B \qquad \text{normal even, } B_2, B_4, B_6 \ldots, \tag{2.10}$$

$$\begin{bmatrix} +1 & +1 \\ -1 & -1 \end{bmatrix} I_C \qquad \text{skew odd, } A_1, A_3, A_5 \ldots, \tag{2.11}$$

$$\begin{bmatrix} -1 & +1 \\ +1 & -1 \end{bmatrix} I_D \qquad \text{skew even, } A_2, A_4, A_6 \ldots. \tag{2.12}$$

In practical dipole magnets all normal odd harmonics are present since the current distribution is slightly different from the ideal cos(θ) shape. Due to fabrication tolerances normal-even and skew harmonics can also arise. In twin-aperture magnets with a common mechanical structure additional field errors are introduced due to (non-symmetric) saturation effects of the iron yoke.

2.2.1 Magnet designs

Two designs of LHC-type dipole magnets are discussed in this thesis (see Table 2.1):

- The Pink Book Dipole magnet[1] -PBD- [LHC, ’91]: the first official design of the bending magnets of the LHC. All experimental results described in chapters 6-8 are based on PBDs and the cables from which the coils are made.
- The White Book Dipole magnet -WBD- [LHC, ’93]: the renewed design for the bending magnets as described in the second concept study for the LHC. The coils are made from smaller cables and operate at a lower field level in an effort to reduce the training as observed in the PBD models. The decrease in the field only slightly reduces the collision

Table 2.1. Survey of the design parameters of two LHC-type dipole magnets. The operating field and current correspond to the indicated collision energy.

		PBD[a]	WBD[b]
Maximum collision energy	TeV	15.4	14
Operating field	T	10	8.65 [c]
Operating current	A	15060	11470
Magnetic length	m	9	13.145
Number of turns of the inner coil per aperture	-	26	30
Number of turns of the outer coil per aperture	-	48	52
Cable width	mm	17	15
Diameter of the aperture	mm	50	56

[a] [LHC '91]
[b] [LHC '93]
[c] In 1994 the operating field was changed to 8.36 T [Perin, ’95]

[1] The names ‘Pink Book’ and ‘White Book’ refer to the colour of the official CERN reports in which the designs of the magnets are described.

energy of the LHC since the effective magnetic length is increased. Results of calculations and simulations on the cables and coils of the WBD magnet are presented in chapters 6-8 in order to envisage the electrodynamic behaviour of the future LHC.

Several aspects of the dipole magnets will be discussed in more detail in the following sections.

2.2.2 Cold mass

The cross-section of the twin-aperture LHC dipole magnet inside its cryostat is shown in Fig. 2.5. The so-called 'two-in-one' structure, in which the two beam channels (or apertures) are enclosed in a common structure, results in an economical and compact geometry.

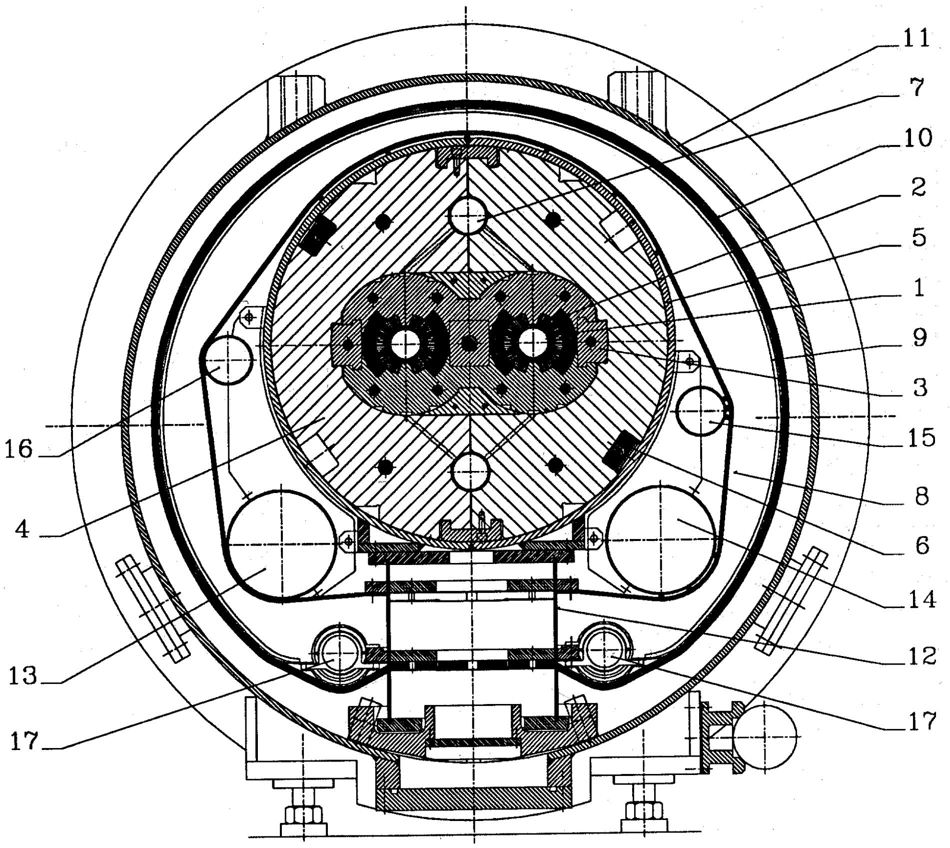

Figure 2.5. Cross-section of an LHC-type dipole magnet within its cryostat [LHC, '91].

1. Beam pipe
2. Coils
3. Collars
4. Yoke
5. Shrinking cylinder
6. Bus bars
7. Heat exchanger
8. Radiative insulation (5 K)
9. Thermal shield (50-70 K)
10. Superinsulation
11. Vacuum vessel
12. Support post
13. GHe pipe (5-10 K)
14. GHe pipe (1.8 K)
15. LHe pipe (2.2 K)
16. He pipe (5 K)
17. Cooling channels (50-70 K)

The part formed by the shrinking cylinder (nr. 5) and the interior are referred to as the cold mass, which is cooled down to a temperature of 1.9 K (or 4.3 K for some test measurements) before excitation. The main components of the cold mass are:

- The inner and outer coils (see Fig. 2.2b), made of superconducting NbTi cable. The characteristics of the cables are given in the section 2.3.
- The aluminium or stainless-steel collars, providing part of the prestress (see section 2.2.3) and defining the exact geometry of the coils.
- The iron yoke, shielding the exterior against the internal field and enhancing the central field in the aperture of the magnet by about 15%.
- The shrinking cylinder, providing part of the prestress and containing the Lorentz forces of about 600 tons/m maximum. It serves to contain the helium of the magnet cold mass and, at the same time, provides structural rigidity and longitudinal support.

2.2.3 Pre-compression of the coils

The support structure compresses the coils radially from the outside which results in an azimuthal compressive stress in the coils. The support has to counteract the Lorentz forces during excitation in order to avoid conductor displacements (i.e. to avoid premature quenching) and coil deformation (i.e. to reduce field errors). The value of the prestress is difficult to calculate due to fabrication tolerances, friction, possible plastic deformation and the different shrinkages of the magnet parts during cool-down. The required compression is about 60 MPa for the outer coil and 80 MPa for the inner coil. During the collaring process, the compressive stress in the coils can be 30-40% higher than the required value in order to obtain a small clearance which would permit the insertion of rods or keys to lock the collars together. Once the press force is released the stress in the coils decreases to a lower value.

The maximum compressive stress in the coils is an important parameter for the interstrand coupling loss since it can lead to deformation of the strand-to-strand contacts and can therefore decrease the contact resistance between strands (see section 4.3).

2.2.4 Field and force distributions

The field distribution over the cross-section of the straight part of the PBD magnet is depicted in Fig. 2.6 and the minimum and maximum values per block are given in Table 2.2. Note that the field varies strongly across the cable width and even reverses its sign in blocks 1 and 2. The consequences of such field variations with respect to the coupling currents are discussed in section 4.4 and chapter 5.

A survey of the minimum and maximum values of the azimuthal stress σ_θ per block is given in Table 2.2. The values are indicative for the actual stress in a coil. During the collaring process the compressive stress in the coils is usually temporarily increased beyond the indicated values in order to lock the collars.

In a twin-aperture magnet the stress is larger in the quadrants near the centre and is slightly smaller in those quadrants near the shrinking cylinder. The compressive stress varies strongly across the cable width, with an average of about 40 MPa in the outer coil and 60 MPa in the inner coil.

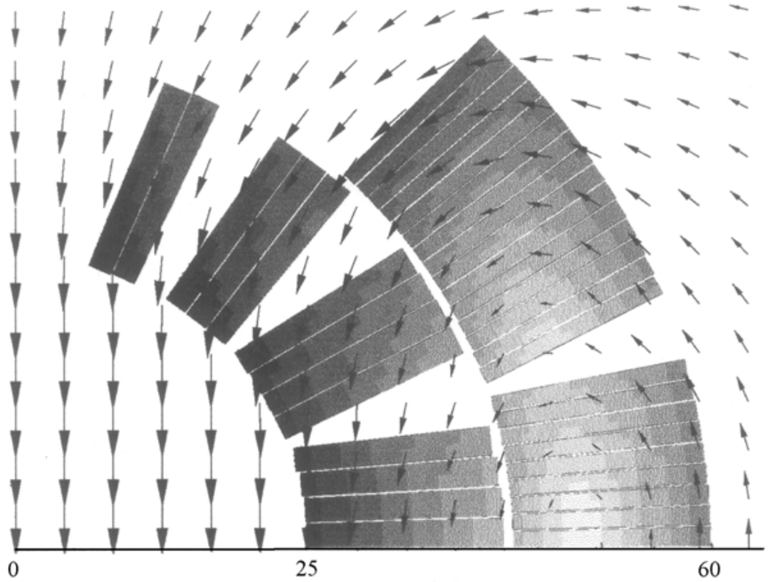

Figure 2.6. Field distribution in one quadrant of the straight part of a PBD magnet [Russenschuck, '93]. The arrows indicate the direction and the magnitude of the field.

The average values increase by about 20 MPa after cool-down. After excitation to 8-10 T the Lorentz force causes the average stress to vary between 105 MPa near the midplane to 50 MPa near the pole. The consequence of such stress variations across the cable width and over the cross-section of the coils on the contact resistance R_c between crossing strands are discussed in section 4.10 and chapter 5.

Table 2.2. Survey of the calculated magnetic field [Russenschuck, '93] and azimuthal stress [Spigo, '94] in each block of the PBD magnet. The minimum and maximum fields correspond to a central field of 10 T. The field $B_\perp$ denotes the field component normal to the wide side of the cables in the block. The stress at 300 K, at 2 K, 0 T and at 2 K, 10 T are characteristic values before and after cool-down and excitation respectively.

Nr. of block	B_x [T]	B_y [T]	$B_\perp$ [T]	$\sigma\theta$(300 K) [MPa]	$\sigma\theta$(2 K, 0 T) [MPa]	$\sigma\theta$(2 K, 10 T) [MPa]
1	0-2.3	-3.1- 4.6	-3.1-4.5	40 (20- 70)	55 (50- 90)	90 (75-110)
2	0.5-5.8	-2.4- 7.6	-3.1-4.3	40 (20- 70)	55 (50- 70)	55 (20- 90)
3	0-1.3	4.5- 9.8	4.5-9.8	55 (0-110)	75 (60- 90)	105 (100-120)
4	-0.1-2.2	5.5- 9.9	4.6-8.7	55 (20- 90)	75 (50-100)	90 (70- 90)
5	0-3.7	7.3-10.1	1.3-6.1	60 (40- 90)	75 (70- 90)	70 (40- 90)
6	0-2.8	7.2-10.2	0.5-4.2	60 (20-140)	80 (70-130)	50 (20- 90)

2.2.5 Superconductor

High-field accelerator dipole magnets with a central field of 8-10 T have coils made of either NbTi or Nb_3Sn superconductors.

NbTi

Up to about 7.5 T, magnets are often cooled by liquid helium at 4.2 K. For higher fields superfluid helium below 2.17 K has to be used as a coolant which requires a more expensive and less efficient refrigeration system. Another drawback is the small heat capacity of all materials at 1.9 K which requires a very good heat exchange with the helium to avoid a temperature increase due to transient energy deposits. The heat capacity C (per unit volume of conductor) of NbTi with copper matrix [Lubell, '83] is:

$$C = (6.8 + 50.6\eta)T^3 + \eta(97.4 + 69.8B)T \quad [\mathrm{Jm^{-3}K^{-1}}] , \tag{2.13}$$

which is about 5 times larger at 4.3 K than at 1.9 K (for a NbTi volume fraction $\eta = 0.35$ and $B = 8$ T). The large heat capacity and heat conductivity of superfluid helium are important advantages for cryogenic stability of the superconductor.

Nb_3Sn

Fields beyond 8-10 T and up to about 18 T at 4.3 K can be attained with Nb_3Sn conductors. One accelerator dipole model magnet with a design field of 11.5 T at 4.2 K [Ouden, den, '94] has been constructed and has reached 11.1 T. Another Nb_3Sn dipole magnet with a design field of 13 T is still under construction [Dell'Orco, '93]. Due to the severe sensitivity of Nb_3Sn to stress and strain [Haken, ten, '94], the coils are made using the 'wind and react process'. This implies that the conductor (with niobium and tin inside) is first wound and then heat-treated (at a temperature of about 700 °C for at least two days) to form the superconducting Nb_3Sn. After the heat-treatment the coils are collared. Although the subsequent impregnation of the coils disables the helium to flow through the voids, the higher heat capacity of the material at 4.3 K could provide a safer operation than when using NbTi. The 'wind and react' process requires that the cable insulation and all other components in the collared coil withstand the reaction temperature.

In some Nb_3Sn conductors 'bridging' occurs, which implies that during the chemical reaction between niobium and tin, filaments link together, thereby increasing the effective filament diameter. Bridging could be a drawback for some Nb_3Sn conductors since it results in larger field distortions and a larger hysteresis loss (see chapter 3).

The formulas presented in this thesis will hold for NbTi as well as for Nb_3Sn cables and magnets unless otherwise specified. However, all experimental results refer to NbTi cables and magnets.

2.2.6 Quenching and protection

The term 'quench' is generally used to denote the irreversible transition from the superconducting to the normal conducting state. A quench is often caused by a local transition of a strand section which generates heat and subsequently causes the other part of the strand and cable to quench. This 'avalanche' process propagates through the strand and cable with a certain propagation velocity of which the value depends on several parameters such as the resistivity of the material, heat transfer, geometry, temperature, field and current. A typical propagation velocity is about 10-50 ms^{-1} for NbTi superconductors.

Many magnets exhibit so-called ‘training’, a process characterised by a quench current that gradually increases with the increasing number of quenches. Training is present if the quenches are caused by displacements of strands or cables which locally heat up the cable (due to frictional energy) or by heat released in the cable surroundings such as epoxy cracking.

A thermal cycle of a (fully) trained magnet often reduces training since many displacements remain irreversible during warm-up and cool-down. Training can be improved by properly clamping the windings (so that the Lorentz force during excitation will not cause any displacement), by improvement of interfaces or impregnations and by enhancement of the cooling capacity of the windings.

When a superconducting magnet quenches, the stored magnetic energy is either dissipated outside the coil or distributed, as much as possible, within the coils to avoid overheating and possibly burning of part of the coil. In magnets with a large stored energy an active system of heaters is used to initiate multiple hot spots in the conductor as soon as a quench is detected, which results in a more global heating of the coils.

In an accelerator ring many magnets are connected in series. In case of a quench, the current is guided around the quenched magnet (by means of diodes) while the remaining series-connected magnets are de-excitated [Coull, 94]. In this case, only the magnetic energy of the quenched magnet is dissipated as heat internally in the magnet. In order to avoid the quench spreading to the other magnets and the diode overheating, the chain of magnets has to be discharged rapidly if there is a quench in one of the magnets. The fast de-excitation is achieved by switching dump resistors in series with the magnets.

The LHC will be divided into 16 sub-units that are powered separately and are therefore electrically independent. The reduction of the coupling loss during de-excitation is, among other things, one of the advantages of such a subdivision. A de-excitation time constant of about 100 s is anticipated for the LHC, which corresponds to an initial field-sweep rate in the centre of the aperture of about -0.084 Ts^{-1}.

During the fast de-excitation, the coils of the series-connected magnets have to remain superconductive. This implies that the generated coupling currents and energy loss during the discharge should not cause the temperature in the cable to increase beyond the current-sharing temperature (see section 2.4).

2.2.7 Operating procedure

The beam is preaccelerated and then injected into the main accelerator at the injection field B_{inj} which is typically a factor of 10 to 20 smaller than the peak field (for LHC: B_{inj}=0.58 T). The field sweep from 0 to B_{inj} can be freely defined since the beam has not yet been injected. A field precycle can be performed to verify the magnet’s characteristics.

Once the beam is injected, which takes about 400 s, the dipole field is ramped up to the operation field. The excitation from injection field to nominal field (8.4 T) for LHC is foreseen to take about 1200 s which corresponds to an average central-field-sweep rate of

0.0066 Ts^{-1}. The field-sweep rate does not have to be constant but may vary during the sweep. At injection as well as at the operating field, the field homogeneity and the field stability in time should meet certain specifications in order to facilitate the field correction.

2.2.8 Beam losses

In high-luminosity colliders a continuous beam loss is present due to the emittance of particles. An actively cooled beam shield, placed inside the aperture, shields the coils from the particles. However, some particles still penetrate into the coils where the energy is absorbed by the conductor (see [Burnod, '89/'91] for a description of this process in LHC). The number of lost protons for LHC that is allowed to maintain the magnet at a sufficiently low temperature can be determined once the energy deposit per incident proton (inside the coil) and the thermal resistance between the coils and the coolant are known. In chapter 8 the latter effect is discussed in detail.

2.2.9 Survey of the model magnets

During the period 1990-1995 several dipole model magnets were constructed in industry and investigated at CERN. A survey of the models is presented in Table 2.3 and the characteristics of the cables are discussed in the next section. Besides the cables, the magnets are slightly different mainly with respect to the materials of the collars, end spacers and outer cylinder.

Table 2.3. Survey of the investigated NbTi dipole model magnets for the LHC (status of march '95). Three 10 m long models that are still under construction are included. The characteristics of the cables of the inner and outer coils of the magnets are presented in the next section (SA = single-aperture magnet, TA = twin-aperture magnet).

Magnet code	Manufacturer	SA/TA	Length [m]	Cable (see Table 2.4) Inner coil	Outer coil	Date of first cool-down
AN1	Ansaldo	TA	1	I-1	O-4	05/91
AN2	Ansaldo	TA	10	I-2	O-3	03/94
AN3	Ansaldo	TA	10	I-6	O-6	07/94
AN4	Ansaldo	TA	10	I-6	O-6	03/95
CE1	CERN	TA	1	I-2	O-3	03/93
EL1	ELIN	TA	1	I-3	O-4	02/91
EL2	ELIN	SA	1	I-3	O-3	08/92
HO1	Holec	TA	1	I-3	O-1	08/91
JS1	Jeumont Schneider	TA	1	I-1	O-2	03/91
KE1[a]	KEK	SA	1	I-5	O-5	05/92
KE2[a]	KEK	TA	1	I-5	O-5	06/93
NO1	Noël	TA	10	I-7	O-7	11/94
AJS1	Alsthom/JS	TA	10			under construction
EH1	ELIN/Holec	TA	10			under construction
NO2	Noël	TA	10			under construction

[a] See [Yamamoto, '93] for more details on the slightly different design.

Either common or separate collars are applied for the two apertures which are assembled with rods and/or keys. These mechanical differences do not significantly contribute to different time-dependent electrodynamic properties of the magnets and are disregarded here but details are presented elsewhere [Bona, '92], [LHC, '93].

The coils of the two magnets manufactured by KEK are made of high keystoned 15 mm wide cables and differ therefore from the other magnets. No wedges are present in these two magnets.

2.3 Strand and cable characteristics

The coils of high field accelerator magnets are often wound from high-current Rutherford-type cables (see Figs. 1.1a and 2.7), mainly to limit the inductance in order to obtain a safe quench protection. Such cables are formed by flattening a hollow tubular cable comprising between 20 and 40 strands. After cabling, the conductors are compacted by rolling in order to increase the overall current density in the coil. Flat NbTi cables can be compacted to filling factors of about 90% without significant damage. During the rolling the dimensional control is important in order to achieve the desired field uniformity.

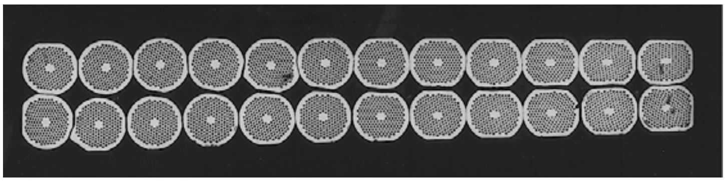

Figure 2.7. Cross-section of a 24-strand Rutherford-type cable with the thick edge on the left and the thin edge on the right. Note the severe deformation of the strands at the thin edge resulting in a large contact area between the strands of the two layers.

The strands are fully transposed with a transposition length (or cable pitch) $L_{p,s}$ which is usually about 6-8 times the cable width w. The cable has a small keystone angle in order to have a more uniform structure of the coils and facilitate the winding of the magnet. The angle is defined as:

$$\alpha_k = \text{atan}\big((h_1 - h_2)/w\big) \quad [\text{deg}] , \tag{2.14}$$

with h_1 and h_2 the thicknesses of the two small sides of the cable. Note the severe deformation of the strands in the cable, in particular at the thin edge, which leads to a large contact area between strands of the top and bottom layers. An increase of the contact area results in a decrease of the contact resistance R_c between the strands of both layers which is one of the key parameters concerning the interstrand coupling loss (see chapter 4).

Particular care is required to provide the cable with an insulation that not only withstands the voltage between turns but is also sufficiently porous to allow permeation of the helium. The insulation has to be strong enough to avoid breakage which could lead to short-circuits between the turns. The insulation is composed of a half-overlapped layer of kapton tape having a thickness of 25 μm and one layer of 125 μm thick glass-fibre tape, pre-impregnated with epoxy resin with spaces of 2.5 mm between successive turns (Fig. 2.8). After winding, the coils are compressed and heat-treated for 2 hours at about 160 °C to cure the resin of the pre-impregnated glass-fibre tape so that adjacent turns adhere to each other. Such a heat treatment under pressure can strongly decrease R_a and R_c, due to plastic deformation of the strands (see section 4.3). The spacing between successive turns of the glass-fibre tape increases the porosity of the coil by forming helium flow channels without affecting the mechanical support between the turns. In and through the channels, the helium comes into direct contact with a large proportion of the cable surface and is likely to penetrate the interior of the cable, thereby providing additional stabilisation due to an increase of the enthalpy.

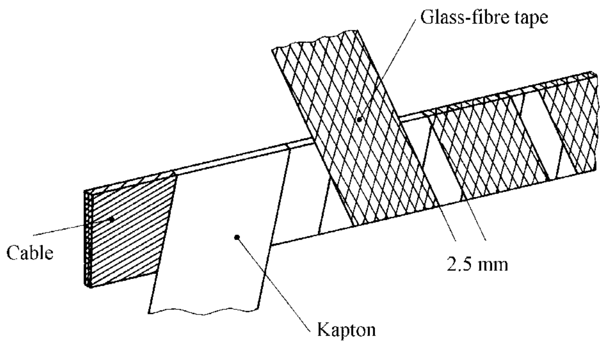

Figure 2.8. Insulation of the cable consisting of a half-overlapped layer of kapton tape with a thickness of 25 μm and one layer of 125 μm thick glass-fibre tape, pre-impregnated with epoxy resin with spaces of 2.5 mm between successive turns.

Due to the large azimuthal pressure on the turns in the coil, which reduces the size of the channels, it is uncertain whether the helium penetrates the channels and the interior of the cable. The maximum temperature of the helium in the interior of the cable should not exceed the transition temperature of 2.17 K, in order to benefit from its high thermal conductivity and low viscosity.

The main parameters of the cables of the LHC dipole model magnets (as specified in Table 2.3) are surveyed in Table 2.4. Note that the width of all the cables is 17 mm except for the cables I-5 and O-5 used in the two KEK dipole magnets. The strands in the cable differ mainly with respect to the filament diameter and the strand coating. The former influences the filament magnetisation (see section 3.2) while the latter affects the contact resistance between crossing strands and therefore the interstrand coupling currents (see section 4.4.1).

The multifilamentary strands consist of NbTi filaments embedded in a copper matrix (see Figs. 2.9a/b). The filaments in the strands are twisted in order to reduce the area enclosed by any two filaments and therefore the interfilament coupling loss in the case of a flux change (see section 3.4).

The main reason for the subdivision into small filaments is the reduction of the filament magnetisation (see section 3.2) which is the main cause of field distortions at weak excitation. Another advantage is the reduction of the energy loss during (de-)excitation.

Table 2.4. The main parameters of the inner (I-1 to I-7) and outer (O-1 to O-7) coil cables. All strands have Nb46.5%Ti filaments.

Name	I-1	I-2	I-3	I-4	I-5
Manufacturer	Alsthom	Alsthom	VAC	VAC	KEK
Dimensions (mm^2)	17.0x2.04/2.50	17.0x2.04/2.50	17.0x2.04/2.50	17.0x2.04/2.50	15x1.88/3.09
Keystone angle (deg)	1.55	1.55	1.55	1.55	4.6
Number of strands	26	26	26	26	22
∅ strand (mm)	1.3	1.3	1.29	1.29	1.39
Cu/SC ratio	1.7	1.6	1.9	1.6	1.6
$L_{p,s}$ (mm)	130	130	130	117	110
∅ filament (μm)	14	5.4	25	4.8	6.0
Number of filaments	3060	21780	900	27954	ca. 21000
$L_{p,f}$ (mm)	25	25	25	25	25
J_C at 8 T, 4.2 K (A/mm^2)	1084	1087	986	938	910
I_C (A) [a]	12350	13364	11288	ca. 12300	
Strand coating	zebra [b]	95%Sn/5%Ag	95%Sn/5%Ag	95%Sn/5%Ag	bare
Soldering	SnPb at one edge	no	no	no	no

Name	I-6	I-7	O-1	O-2	O-3
Manufacturer	LMI	Alsthom	ABB	Alsthom	Alsthom
Dimensions (mm^2)	17.0x2.04/2.50	17.0x2.04/2.50	17.0x1.32/1.67	17.0x1.30/1.65	17.0x1.30/1.65
Keystone angle (deg)	1.55	1.55	1.2	1.2	1.2
Number of strands	26	26	40	40	40
∅ strand (mm)	1.29	1.29	0.84	0.83	0.84
Cu/SC ratio		1.7	1.8	1.8	1.8
$L_{p,s}$ (mm)	120	130	132	95	100
∅ filament (μm)	7.8	4.8	14	9.5	5.1
Number of filaments	ca. 10500	26268	1230	2550	9438
$L_{p,f}$ (mm)	25	25	25	25	25
J_C at 8 T, 4.2 K (A/mm^2)				1136	
I_C (A) [a]			16350	16040	16200
Strand coating	95%Sn/5%Ag	95%Sn/5%Ag	95%Sn/5%Ag		
Soldering	no	no			

Name	O-4	O-5	O-6	O-7
Manufacturer	LMI	KEK	LMI	VAC
Dimensions (mm^2)	17.0x1.33/1.65	15.0x1.10/1.55	17.0x1.30/1.65	17.0x1.30/1.65
Keystone angle (deg)	1.1	1.7	1.2	1.2
Number of strands	40	37	40	40
∅ strand (mm)	0.84	0.79	0.84	0.84
Cu/SC ratio	1.8	1.8		1.75
$L_{p,s}$ (mm)	130	110	120	100
∅ filament (μm)	16	6.0	7.8	4.8
Number of filaments	ca. 1000	ca. 6000	ca. 4000	10164
$L_{p,f}$ (mm)	25	25	25	25
J_C at 8 T, 4.2 K (A/mm^2)		1040		
I_C (A) [a]	17680	13766		
Strand coating		bare	95%Sn/5%Ag	95%Sn/5%Ag
Soldering	SnPb			

[a] at 8 T, 4.2 K for I-1 to I-7, and at 6 T, 4.2 K for O-1 to O-7
[b] see section 4.6

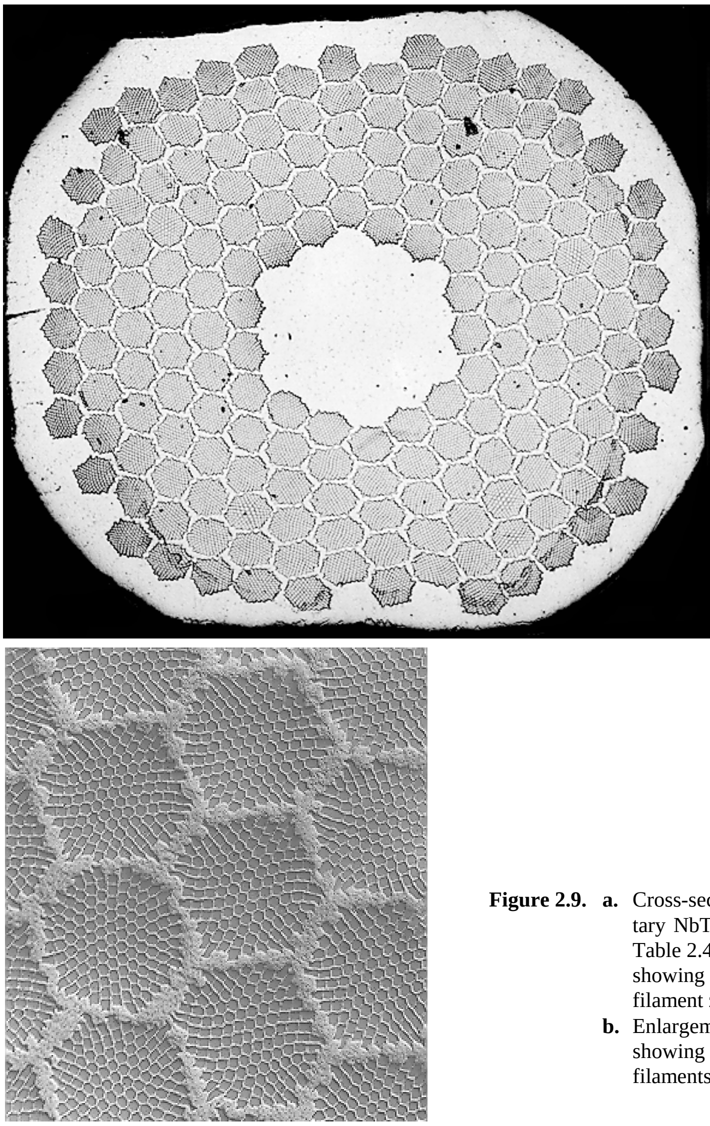

Figure 2.9. **a.** Cross-section of a multifilamentary NbTi strand (number I-2, see Table 2.4) with 21780 filaments, showing the central core, the filament zone and the outer shell.
b. Enlargement of part of the strand showing the hexagonal bundles of filaments.

The stability of the strand in face of local thermal disturbances also benefits from the subdivision into small filaments. If a disturbance causes the temperature of a filament to rise locally beyond the critical temperature, the matrix can rapidly conduct the heat and transfer the current of the filament to adjacent filaments. The electrical resistivity of the matrix should therefore be small, especially in the longitudinal direction. The resistivity ρ_{mat} of the matrix at liquid-helium temperature can be expressed by:

$$\rho_{mat} = \rho_{mat,0}\left(1+\alpha_m|B|\right) \quad [\Omega\text{m}] , \tag{2.15}$$

in which $\alpha_m|B|$ represents the increase of the resistivity by magnetoresistance which is inherent to metals. Technical values of $\rho_{mat,0}$ and α_m for copper are about $1\text{-}2{\cdot}10^{-10}$ Ωm and 0.5 respectively. The RRR-value (Residual Resistivity Ratio) gives the ratio between the resistivity at 300 K and at 4 K for zero field and is generally about 50-200 for practical NbTi superconductors.

A common lay-out of the cross-section of a NbTi strand consists of the following three concentric layers (see Fig. 2.9a):

– a central core of normal-conducting material,
– a ring filled with many thin filaments embedded in a matrix,
– an outer shell of normal-conducting material.

The outer shell is required to facilitate the wire production. The purpose of the normal-conducting core (and shell as well) is to maintain the required Cu/SC ratio for stability, since an empirical criterion for the filament spacing to filament diameter is about 0.15-0.20 [Green, '87].

The strands can be coated to increase R_a and R_c and therefore reduce the interstrand coupling currents and power loss (see chapter 4). Besides coatings, internal barriers in the strand or resistive barriers between the top and bottom layers of flat cables also enhance the contact resistances.

2.4 The $I_C\,(B, T)$ relation

The critical current I_C in a superconductor is a function of the field B and temperature T. The $I_C\,(B, T)$ relation for NbTi can be described by the following formulas where the field direction is perpendicular to the current. At constant temperature the I_C-B relation is expressed by means of the Kim relation [Kim, '62]:

$$J_C = J_0 B_0 / \left(B_0 + |B|\right) \quad [\mathrm{Am}^{-2}] \text{ or: } I_C = I_0 B_0 / \left(B_0 + |B|\right) \quad [\mathrm{A}] \quad \text{for } |B| < B^*, \tag{2.16}$$

with J_0, I_0 and B_0 temperature-dependent parameters. The Kim relation holds for most practical NbTi superconductors with B^* of about 3 T. The dependence of I_C on the field component parallel to the strand axis is not considered here since the relation is not well-known. A linear relationship for higher field is assumed (at constant temperature):

$$I_C = I_{C,0}\left(1 - C_0|B|\right) \quad [\mathrm{A}] \quad \text{for } |B| > B^*. \tag{2.17}$$

The temperature dependence of eq. 2.17 for NbTi with a volume fraction of about 45-50%Ti is expressed by the following empirical scaling law [Lubell, '83]:

$$I_C = \left(C_1 - C_2|B|\right)\left(1 - \frac{T}{T_C\,(B, I=0)}\right) \quad [\mathrm{A}] \quad \text{for } |B| > B^*, \tag{2.18}$$

with the critical temperature or current-sharing temperature:

$$T_C\,(B, I=0) = 9.2\left(1 - |B|/14.5\right)^{0.59} \quad [\mathrm{K}]. \tag{2.19}$$

The linear relation between I_C and T is valid for temperatures higher than about 2-2.5 K. The constant 14.5 T (i.e. the critical field at 0 K and 0 A) has to be changed to about 14.8 T for fields larger than 10 T. In chapter 8 the linear relation is extended to temperatures of 1.9 K, which has no significant effect on the analysis of the ramp-rate limitation of magnets.

The I_C-B relation at several temperatures is shown in Fig. 2.10. Also a characteristic ‘load line’ is included in the figure, which indicates the relation between the transport current in the cable and the peak field in the coil. In magnets with grading of the current density, each coil has a load line. The point of intersection of the load line and the $I_C(B, T)$ relation indicates the maximum operating field and current at a temperature T. In magnets the operation field is about 20% lower than the critical field. The *temperature margin* is then defined as the difference between the operating temperature and the current sharing temperature.

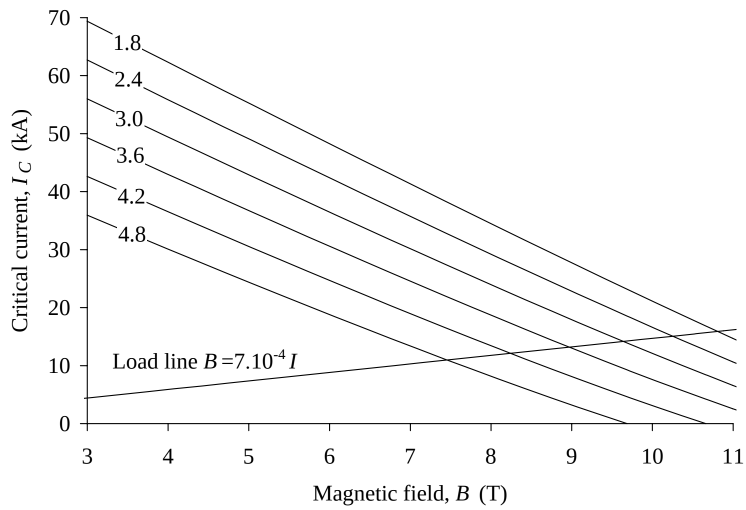

Figure 2.10. The I_C-B relation of NbTi at several temperatures (1.8, 2.4, 3.0, 3.6, 4.2 and 4.8 K from top to bottom) according to eqs. 2.18 and 2.19 in the field range between 3 and 10 T. The constants C_1 and C_2 are taken to be $11.3{\cdot}10^4$ A and $7.8{\cdot}10^3$ AT^{-1} respectively.

The unknown parameters I_0 and B_0 in the Kim relation are usually determined by means of a magnetisation measurement (see also section 3.3), while the temperature-dependent constants $I_{C,0}$ and C_0 in eq. 2.17 are often extracted from a voltage-current measurement.

The current and field of a magnet cannot be varied independently, so that only one $I_C(B)$-value can be deduced at a certain temperature. The parameters C_1 and C_2 can then be deduced from the quench current (after training) at two different temperatures (e.g. 1.9 and 4.3 K). This is not possible if the training procedure is not completed or if the magnet is only operated at one temperature. In this case additional voltage-current measurements on a piece of cable, identical to the cable that is used in the coils, are required to estimate the parameters C_1 and C_2.

2.5 Conclusions

Several aspects affecting the time-dependent electrodynamic behaviour of a coil are inherent to the design of the accelerator dipole magnet itself and are surveyed here.

- The need for a low inductance, in order to have a safe quench protection, requires a high-current cable. In order to increase the overall current density, coil are wound from multistrand Rutherford-type cables which are compacted to filling factors of about 90%. The combination of wide cables with a good contact between the strands enhances the coupling currents and power loss considerably (see chapter 4). In order to reduce the interstrand coupling currents, the strands are twisted. A further reduction of the coupling currents can be obtained by applying a coating on the strands, an internal resistive barrier in the strand or a resistive layer between the strands.

- The heat-treatment, in order to cure the resin of the pre-impregnated glass-fibre tape of the cable insulation, often results in a smaller R_c (see section 4.3), especially if the heat treatment is applied under pressure.

- A further reduction of R_c is inherent to the large stresses in the coils. These stresses are due to the Lorentz force during excitation as well as the large prestress that is required to avoid conductor displacements.

- The keystone of the cable results in a strong variation of R_c across the cable width.

- The performance of the magnet is improved by grading of the current density between the layers. This requires cable-to-cable connections with a small resistance to minimise the resistive loss. The local reduction of R_c introduces boundary-induced coupling currents during a field sweep (see chapter 5).

- The field perpendicular to the wide side of the cable decreases strongly in the coil ends where the cable bends around the beam pipe. These local variations in the field also provoke boundary-induced coupling currents during and after field sweeps.

The excitation of the LHC dipole magnets from the injection field (ca. 0.58 T) to the nominal field (ca. 8.4 T) is anticipated to take about 1200 s, which corresponds to an average central-field-sweep rate of about 0.0066 Ts^{-1}. In the case of a quench in a coil, the series-connected magnets have to be rapidly discharged. The time constant of the fast de-excitation is about 100 s which corresponds to an initial field-sweep rate of about -0.084 Ts^{-1} maximum.